Spectrochimica Acta Part A: Molecular and Biomolecular Spectroscopy 286 (2023) 122020

Contents lists available at ScienceDirect

Spectrochimica Acta Part A:
Molecular and Biomolecular Spectroscopy

journal homepage: www.journals.elsevier.com/spectrochimica-acta-part-a-molecular-and-biomolecular-spectroscopy

Spectroscopic characterization of different protonation/deprotonation states of Barbaloin in aqueous solution

Fernanda Lima Matos [a], Evandro L. Duarte [a], Gabriel S. V. Muniz [a,b], Erix Alexander Milán-Garcés [a], Kaline Coutinho [a], M. Teresa Lamy [a], Antonio R. da Cunha [a,c,*]

[a] Instituto de Física, Universidade de São Paulo, CEP 05508-090, Cidade Universitária, São Paulo, Brazil
[b] Instituto de Química, Universidade de Brasília, CEP 70910-900, Campus Universitário Darcy Ribeiro, Brasília, Brazil
[c] Universidade Federal do Maranhão, UFMA, Campus Balsas, CEP 65800-000, Maranhão, Brazil

HIGHLIGHTS

- Characterization of Barbaloin optical absorption and fluorescence spectra at different *pH* values.
- Through both optical absorption and fluorescence spectroscopy, two pK_a values for Barbaloin in aqueous solution were found.
- Characterization of optical absorption and fluorescence spectra of Barbaloin degraded products at high *pH*.
- Discussion about the best way to do a reliable *pH* titration with Barbaloin.
- Assignment of Barbaloin protonation/deprotonation sites in water by quantum mechanical calculations using DFT.

GRAPHICAL ABSTRACT

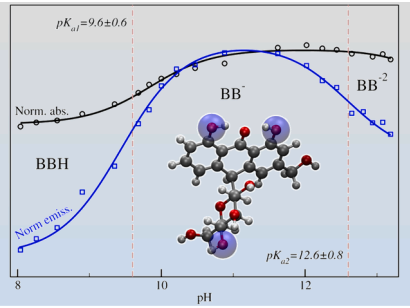

ARTICLE INFO

Keywords:
Barbaloin
UV/Visible spectroscopy
Fluorescence spectroscopy
Protonation and deprotonation
Anthraquinones

ABSTRACT

Barbaloin (10–glucopyranosyl–1,8–dihydroxy–3–(hydroxymethyl)–9(10*H*)–anthraquinone: aloin A), present in Aloe species, is widely used in food, cosmetic and pharmaceutical industries. Here we characterize its optical absorption and emission spectra in aqueous solution at different *pH* values. Through *pH* titration, using both absorption and fluorescence spectroscopy, two pK_a values for Barbaloin were determined: $pK_{a1} = 9.6 \pm 0.6$ and $pK_{a2} = 12.6 \pm 0.8$. These acidity constants were found to be higher than those found for Emodin, a similar molecule which lacks the sugar moiety present in Barbaloin. Performing quantum mechanical calculations for non-ionized, singly, doubly, and triply deprotonated forms of Barbaloin in vacuum and in water, we assigned the positions of the site for the first and third deprotonation in the anthraquinone group, and the second deprotonation in the glucose group. The instability of Barbaloin in high *pH* solutions is discussed here, and the optical absorption and fluorescence spectra due to products resulted from Barbaloin degradation at high *pH* is well separated from the Barbaloin original spectra. Biological fluids have specific *pH* values to maintain homeostasis, hence determining the pK_a of Barbaloin is important to evaluate the mechanism of action of this drug in different parts of an organism as well as to predict pharmacological relevant parameters, such as absorption, distribution, metabolism, and excretion.

* Corresponding author.
E-mail addresses: fernanda.matos@usp.br (F. Lima Matos), elduarte@usp.br (E.L. Duarte), gabriel.vignoli@unb.br (G. S. V. Muniz), garces@usp.br (E. Alexander Milán-Garcés), kaline@if.usp.br (K. Coutinho), mtlamy@usp.br (M. Teresa Lamy), antcunha@if.usp.br (A.R. da Cunha).

https://doi.org/10.1016/j.saa.2022.122020
Received 17 May 2022; Received in revised form 25 September 2022; Accepted 17 October 2022
Available online 22 October 2022
1386-1425/Published by Elsevier B.V.

1. Introduction

Barbaloin (10–glucopyranosyl–1,8–dihydroxy–3–(hydroxymethyl)–9(10*H*)–anthraquinone: aloin A) (Fig. 1) is the most important phyto-constituent of Aloe species, widely used in food, cosmetic and pharmaceutical industries [1 2 3 4]. It is a natural anthraquinone glycoside, found in the outer rind of the aloe plant. It can constitute up to 30% of aloe plants dried leaf exudates [1], and is considered to be a part of their defense mechanisms against herbivores [5 6]. This anthraquinone is known for its biological activities, such as antiviral [7 8], antioxidant [9 10 11], anti-inflammatory [12 13], and anti-cancer [14 15] activities, and as an inhibitory agent [16 3]. Previous studies revealed that Barbaloin has a much higher inhibitory efficacy in histamine release from human mast cells [17] than some anti-inflammatory drugs [18].

In vivo studies have shown that orally administered Barbaloin is poorly absorbed, but metabolized by intestinal micro flora into Aloe-emodin [19], known as the reduced form of Barbaloin, which is very stable and more readily absorbed [20 3]. This anthraquinone has demonstrated efficacy in several cancer types, including human lung carcinoma [21 22], hepatoma [23 24], breast [25 26], colon carcinoma [27 28] and leukemia [29 30]. Aloe-emodin was also reported to induce apoptosis in human gastric carcinoma cells [31], lung carcinoma cells [21] and hepatoma cells [24 23]. The toxicological properties of both Barbaloin and Aloe-emodin have been investigated in many studies, which revealed that both molecules display selective cytotoxic activity against cancer cells [14 15 32 33 34 35 36]. On the other hand, they show almost no harmful effect or toxic potential on normal cells [34]. Despite evidence suggesting that Barbaloin and Aloe-emodin can be used in many cancer treatments, there is not enough information to establish a molecular mechanism that explains how these anthraquinones affect cancer cells. One important path towards this understanding is the study of the interaction of the anthraquinone with the tumor cell membrane. In previous studies, it was shown that Barbaloin strongly affects the structural properties of different lipid model membranes at physiological *pH* [37 38], possibly due to hydrogen bonds between the anthraquinone and the lipid head groups [38]. But the importance of the anthraquinone's hydroxyl groups (Fig. 1) in the lipid interaction is still not clear.

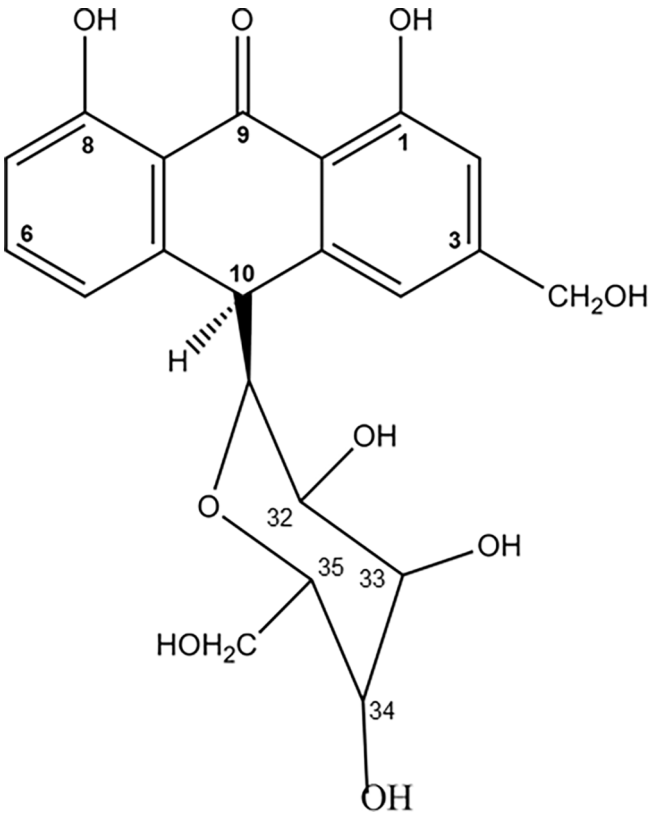

Fig. 1. Chemical structure ($C_{21}H_{22}O_9$) and atomic numbering of Barbaloin in its neutral form (BBH).

The protonation/deprotonation processes of several anthraquinones, such as Emodin, Physcion, Chrysophanol, Aloe-emodin, and Rhein were experimentally analyzed and their acidity constants were determined [39 40 41 42 43 44 45]. In a previous work [46], it was demonstrated that the red shift in the absorption spectrum of Emodin (1,3,8-trihydroxy-6-methyl-9,10-anthraquinone), accompanied by a noticeable change in the color of the sample with increasing *pH* value is due to deprotonation processes of the anthraquinone in solution. A stepwise dissociation of three protons at $pK_{a1} = 8.0$, $pK_{a2} = 10.9$, and $pK_{a3} > 13.8$ was demonstrated, with pK_a values obtained using UV/Visible spectrophotometric titration (ST) technique. Barbaloin has the same core structure of Emodin, but different peripheral functional groups, the two main groups being the glucose moiety and the hydroxymethyl group, attached to C-10 and C-3, respectively (see Fig. 1). Therefore, varying the *pH* from acidic to alkaline in aqueous solution the stepwise dissociation of Barbaloin may be different from that of Emodin, although glucose should remain protonated in this *pH* range [47].

It is important to have in mind that biological fluids, in different parts of an organism, display different *pH* values, necessary for their specific functions [48 49]. Therefore, the knowledge of the acidity constants of biological relevant dye molecules is fundamental for the study of their action, as different protonated species will be present in the different fluids [50 51 52].

The optical absorption spectrum of Barbaloin has been used to identify and to quantify the molecule in aloe vera and in some commercial products [53 54 55]. Dried Barbaloin is a brownish-yellow amorphous solid at room temperature, water soluble under different *pH* conditions, and known to give off yellow fluorescence in alkaline solutions [56]. In water under acidic conditions, and in usual organic solvents, it displays a broad optical absorption spectrum band between 310 and 420 nm, with maximum absorption wavelength (λ_{max}) varying from 352 nm in water to 366 nm in benzene, resulting in a yellow-whitish color. Under alkaline conditions, this band is red shifted to 320–500 nm depending on the solvent, yielding a lively-yellow color. Moreover, in some solvents, such as methanol and acetonitrile, this broadband contains several peaks, suggesting a band splitting. The optical absorption spectra and the main absorption maximum of the Barbaloin in various solvents, under both acidic and alkaline conditions, are shown in the Supplementary Material (Fig. 1SM and 2SM).

Factors such as *pH*, temperature and light exposition have been reported to affect the stability of Barbaloin in solution [57 58 59 60 61 62 63], suggesting that this anthraquinone has high stability at acidic *pH*, but faster and non-reversible degradation at alkaline *pH* values.

In this context, we studied the protonation/deprotonation process of Barbaloin in aqueous solution, using experimental techniques and theoretical quantum mechanics calculations. With optical absorption and fluorescence spectroscopic titration techniques we determined the pK_a values of Barbaloin in water (the pK_a value of an isolated titratable site, here called acidity constant, is equal to the *pH* at which the deprotonation probability of this site is 1/2). The reversible effects of protonation/deprotonation on Barbaloin spectra were identified by comparing two titration methodologies: acid to alkaline (up-titration) and alkaline to acid (down-titration). We report a gradual dissociation of two protons in the *pH* range of 2 to 13, and a loss of stability of Barbaloin at alkaline *pH*. We obtained accurate experimental pK_a values for the molecule, which, to the best of our knowledge, are not available in the literature. In addition, the assignment of the Barbaloin protonation/deprotonation sites in aqueous solution was successfully predicted by quantum mechanical calculations using Density Functional Theory [64 65].

2. Experimental

2.1. Reagents

Barbaloin (Aloin A, Fig. 1), Hydrochloric acid (12 M), Sodium hydroxide, Methanol, Ethanol, 2-Propanol, Acetonitrile, DMSO, Acetone, Dichloromethane, Chloroform, Dioxane, and Benzene (all spectroscopic quality) were purchased from Sigma–Aldrich Co. (St. Louis, MO, USA), and used without further purification. Milli-Q water was used throughout.

2.2. Sample preparation

A 5 mM Barbaloin stock solution was prepared in ethanol/methanol (4:1, v:v) and used in all experiments. Aliquots of the stock solution were separated in amber glass vials, using a calibrated micropipette, dried under a stream of N_2 gas, and left under reduced pressure for a minimum of two hours to remove organic solvent traces. To perform the spectroscopic titration experiments, aqueous samples at two different *pH* values were prepared: an alkaline at $pH \sim 13$, and an acidic at $pH \sim 2$, by the addition of NaOH and HCl, respectively. Then, formed Barbaloin films were dissolved in those two different *pH* aqueous solutions, to a final concentration of 0.025 mM. All samples were prepared with Milli-Q water, kept in amber glass bottles, and vortexed for approximately 30 s before use.

2.3. Spectroscopic titration (ST)

Optical absorption experiments were carried out on a UV/Visible spectrophotometer (Varian Cary 50, Santa Clara, CA, USA) equipped with a Cary Peltier thermostat. Samples were placed in a quartz cuvette (4 × 10 mm) with an optical absorption path of 10 mm, and measurements were performed at 25 °C.

Steady-state fluorescence emission spectra were recorded on a fluorescence spectrometer (Varian Eclipse, Santa Clara, CA, USA). Samples were placed in a quartz cuvette (4 × 10 mm), with an optical pathway for excitation of 4 mm, and all measurements were carried out at 25 °C, controlled by a Cary Peltier thermostat. Barbaloin samples were studied at two excitation wavelengths, 352 and 388 nm, corresponding to their major absorption bands in acid and alkaline aqueous solutions (see Fig. 2). The inner filter correction was applied to all the fluorescent emission spectra [66 67].

Titration experiments were performed as previously described [46 68]. From both acidic ($pH \sim 2$) and alkaline ($pH \sim 13$) Barbaloin aqueous solutions, intermediate *pH* samples were prepared by successive addition of small aliquots (around 5 up to 50 μL) from one solution to the another. Namely, two different procedures were used: (i) up-titration, from acidic to alkaline *pH* values and, (ii) down-titration, from alkaline to acidic *pH* values. Each procedure was performed with three independent samples.

Absorbance and fluorescent emission measurements were performed using the same Barbaloin sample, with the fluorescence emission acquired right after the absorption spectrum. Before measurement, samples were homogenized by vigorous vortexing, and its *pH* was measured with a Mettler Toledo (Seven Easy) *pH*-meter.

2.4. Determination of acidity constants

The acidity constants (pK_a) of Barbaloin in aqueous solution were determined by the spectroscopic titration (ST) curve analysis as previously described [46]. Here, this method was applied to both optical absorption and fluorescent emission titration curves, with the appropriate modifications. The optical absorption ST curves were obtained by selecting the absorbance at two wavelengths, 352 and 388 nm, as a

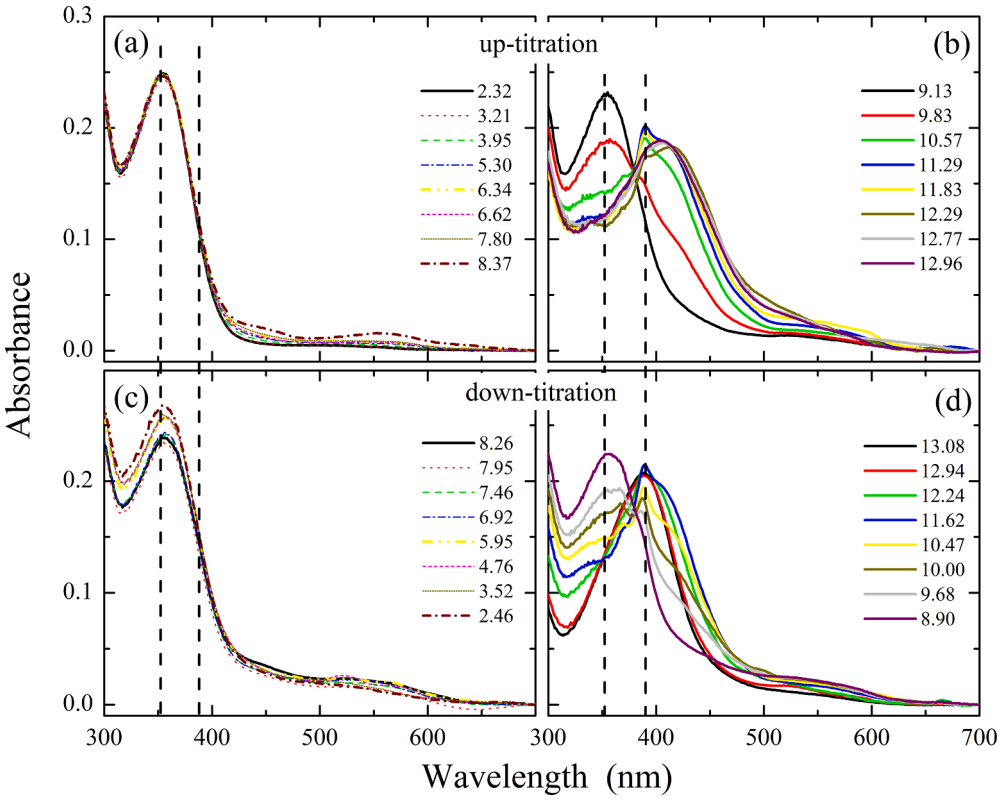

Fig. 2. Barbaloin (0.025 mM) optical absorption spectra in aqueous solution at different values of *pH*. For the sake of clarity, the spectra are separated into two regions, low *pH* region (a) and (c), and high *pH* region (b) and (d), for both up-titration (a) and (b) and down-titration (c) and (d). Dashed lines indicate the wavelengths 352 and 388 nm.

function of the *pH*. For fluorescence emission ST curves, the emission wavelength 546 nm was selected as a function of the *pH*. The pK_a values were determined by the best fitting of these ST curves using the Eq. (1),

$$I = I_0 + \sum_{i=1}^{n} I_i \left(\frac{10^{\pm(pH - pK_{ai})}}{1 + 10^{\pm(pH - pK_{ai})}} \right) \quad (1)$$

where, I is the total absorbance or fluorescence emission intensity measured at a given wavelength, n is the number of non-interacting deprotonation sites of the molecule, and I_0, I_i are constants to be determined by the fitting of the ST curves. It is worth mentioning that the number n is not known beforehand, but it is indicated by the ST curves via trial and error, being the smallest whole number that allows an adequate fitting, as discussed below (see Fig. 6 and Table 1). Note that, in a specific wavelength, if I increases in a certain range of *pH*, then the positive sign (+) is chosen to describe an increasing sigmoidal ST curve, but if I decreases, the negative sign (−) is used.

3. Theoretical calculations

The neutral form of Barbaloin (BBH, see Fig. 1) and all the possible deprotonated forms with deprotonation sites up to 3 (BB^{-1}, BB^{-2}, and BB^{-3}) had initially their geometry optimized for the structures in vacuum, and the vibrational frequencies calculated with quantum mechanics (QM), using Density Functional Theory (DFT) [69] with the B3LYP exchange–correlation functional [70 71] and Pople basis set functions, 6–311++G(d,p) [72]. This method has been successfully used for Barbaloin [73], Emodin [46], and other anthraquinones, providing good results in calculating various electronic properties. The obtained vacuum geometries were reoptimized in aqueous solution, followed by frequency calculations. Non-imaginary frequencies were found in vacuum and in water, confirming that all obtained structures correspond to equilibrium geometries. The solvent was treated by the polarizable continuum model (PCM) [74] with the same level of QM calculation, B3LYP/6–311++G(d,p). Previously, we compared values of protonation/deprotonation free energy variations and pK_a obtained with PCM and explicit solvent models with molecular mechanics simulations and free energy perturbation theory for Emodin in aqueous solution and concluded that the PCM is a good approximation for identifying protonation/deprotonation sites for this type of molecule [46]. The protonation/deprotonation sites in Barbaloin were assigned by comparing the Gibbs free energy of isomers with the same quantity of deprotonation sites. The Gibbs free energies of all isomers in vacuum and in aqueous solution were calculated considering the electronic energy of the system and the corrections of zero-point energy, thermal and enthalpy at the same level of QM calculation. All QM calculations were performed with Gaussian 09 program [75].

4. Results and discussions

4.1. Absorption and emission spectroscopic titrations

Spectroscopic titration experiments were performed with Barbaloin in water at 0.025 mM, prepared as described in Materials and methods. Accordingly, two different *pH* titrations were performed, with *pH* ranging from ~ 2 to ~ 13 (up-titration) and from ~ 13 to ~ 2 (down-titration). For the sake of clarity, Fig. 2 shows the absorption spectra of Barbaloin separated into two different *pH* regions (the low-neutral *pH* region (Fig. 2a, c), from ~ 2 to approximately 8, and the high *pH* region (Fig. 2b, d), from ~ 8 to approximately 13, for the two *pH* cycles. In the low *pH* region, a broadband centered at 352 nm can be observed, and the absorption spectra display little dependence upon *pH* variation (Fig. 2a and 2c), hence suggesting the absence of protonation/deprotonation processes along that *pH* range. Therefore, it possibly corresponds to the neutral fully protonated Barbaloin species.

For the high *pH* region (Fig. 2b, d), Barbaloin optical absorption spectrum is very sensitive to the medium *pH* value, indicating the presence of protonation/deprotonation processes along that *pH* range. Moreover, the absorption spectra were found to be somehow different

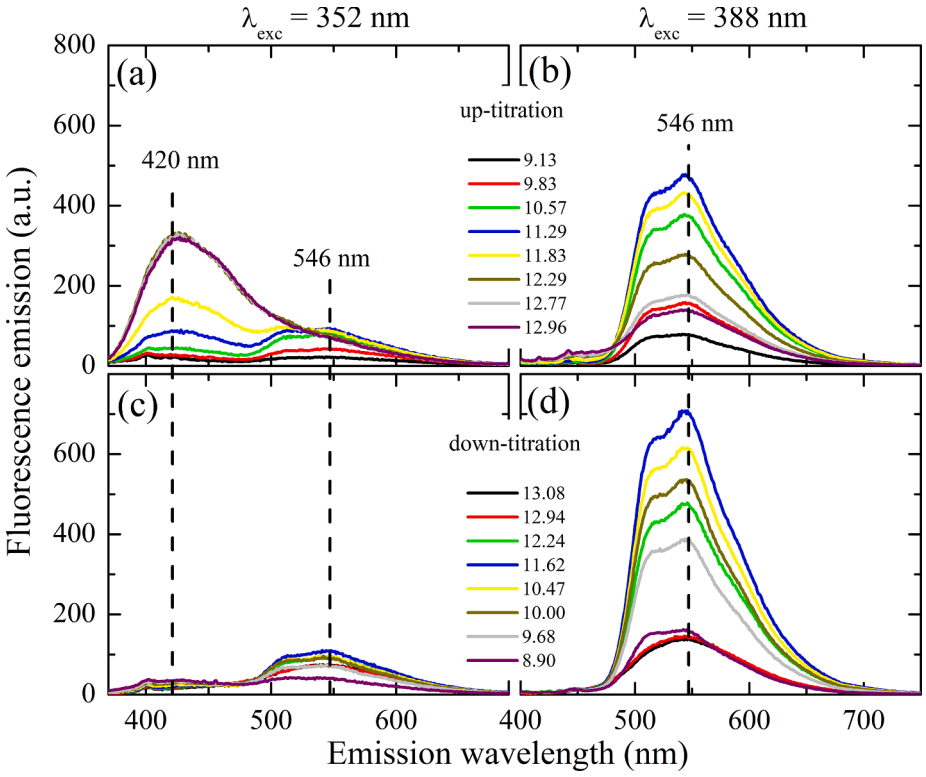

Fig. 3. Barbaloin (0.025 mM) fluorescence emission spectra in aqueous solution at different values of *pH*, for both up-titration (a and b) and down-titration (c and d). Barbaloin samples were excited at 352 (a and c) and 388 nm (b and d). Dashed lines are guides for the eyes only, as discussed in the text.

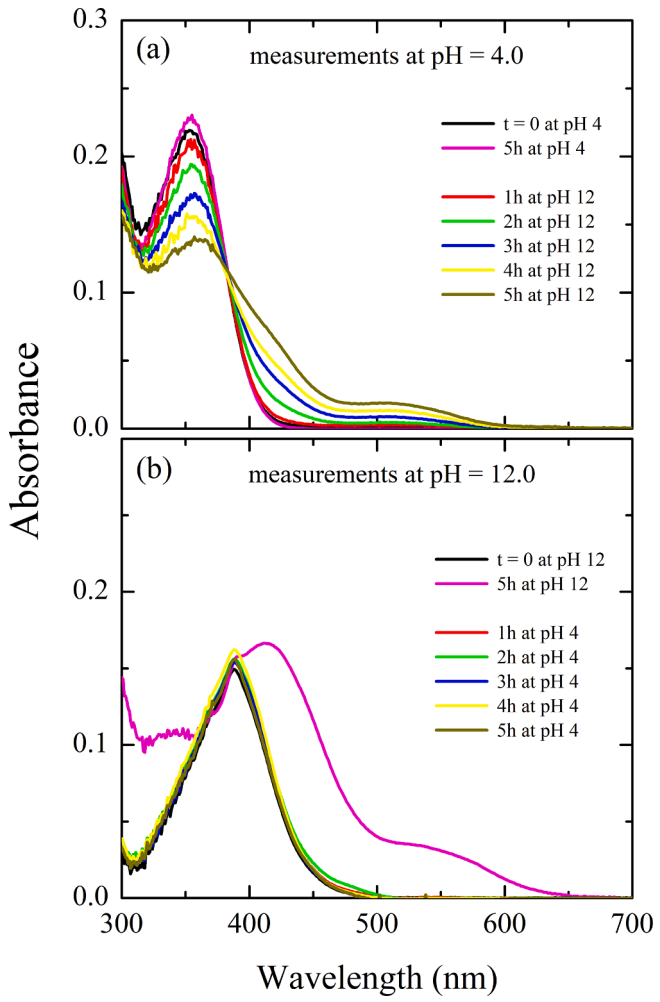

Fig. 4. Barbaloin (0.025 mM) optical absorption spectrum measured with samples at *pH* 4.0 (a) and *pH* 12.0 (b). Spectra measured immediately after preparing the sample at *pH* 4 (black line in a) and at *pH* 12.0 (black line in b). Spectrum measured at *pH* 4.0 after incubating the sample for 5 h at *pH* 4 (pink line in a), and spectrum measured at *pH* 12.0 after incubating the sample for 5 h at *pH* 12 (pink line in b). The other spectra (lines red, green, blue, yellow and dark yellow) were obtained after incubating the sample for the given time at *pH* 12.0, and measured at *pH* 4.0 (a), or at *pH* 4.0 and measured at *pH* 12.0 (b), as stated.

depending on the *pH* cycle, up- or down-titration. Differences can be observed in the wide band between 450 and 630 nm with maximum absorption wavelength around 530 nm in the high *pH* region, which is more pronounced in the spectra obtained for up- than for down-titration. Other differences although more subtle can also be seen in the band located around 388 nm: for the spectra in the up-titration it is redshifted by 17 nm compared to those obtained in the down-titration. Those differences can be better observed in Fig. 3SM.

To the best of our knowledge, such spectra along the high-*pH* region are so far unavailable in the scientific literature. However, in the low-*pH* region, the obtained result is in good agreement with Barbaloin spectrum measured in aqueous solution at *pH* 7.4 [55 76 77].

To better understand the *pH* dependence of Barbaloin in aqueous solutions, fluorescence steady-state measurements were performed, for both up- and down-titrations. The fluorescence emission can bring important information about deprotonation and degradation processes that are not easily observed with optical absorption in many molecular systems. Indeed, the appearance or quenching of fluorescence provides valuable information on the nature of these processes in solution [78 79 80]. Therefore, steady-state fluorescence measurements were performed using the same samples and experimental conditions applied to the absorption titration experiment. Samples were excited at 352 and 388 nm, based on the absorption results: they are approximately the maximum values of the optical absorption bands at low and high *pH* values, respectively (see Fig. 2).

The emission spectrum of Barbaloin in water along the low *pH* region, for both up- and down-titration cycles, showed very low fluorescence intensity for the excitation at the two wavelengths, 352 and 388 nm (see Supplementary Material, Fig. 4SM a, b, e and f). These spectra are in reasonable agreement with previous measurements reported in the literature [77].

Fluorescence emission of Barbaloin in water along the high *pH* region is presented in Fig. 3. When excited at 352 nm, the anthraquinone presents a quite different behavior for up and down *pH* cycles. The main difference is the increasing band around 420 nm as the *pH* increases (Fig. 3a), which is not observed for the down-titration cycle (Fig. 3c), indicating that this band is not reversible, hence not due to deprotonation process. On the other hand, if excited at 388 nm, Barbaloin emission displays somehow similar behaviors along the two titration cycles (Fig. 3b and 3d), with a broad band around 546 nm gradually increasing as the *pH* varies from 9.0 to 11.0, and then decreasing at *pH* values above 11.0.

4.2. *Reversibility analysis of absorption and emission optical spectra*

To better understand the differences among up- and down-titrations, the following experiments were performed. Barbaloin solutions (0.025 mM) were prepared at *pH* 4.0 and 12.0. Aliquots of these solutions were immediately separated after preparation, and their absorption and emission spectra acquired: at *pH* 4.0 $t = 0$ spectrum in Fig. 4a (absorption) and in Fig. 5a, b (emission), and at *pH* 12.0, $t = 0$ spectra in Fig. 4b (absorption) and in Fig. 5c, d (emission). Those aliquots were left on the bench for 5 h. After that, their *pH* was checked, corrected if necessary, and their absorption and fluorescence spectra registered, the pink spectra in Figs. 4 and 5, for sample absorption and emission, respectively, Fig. 4a and 5a and b, for the sample prepared and kept at *pH* 4.0, and Fig. 4b and 5c and d, for the sample prepared and kept at *pH* 12.0. Moreover, part of the sample prepared at *pH* 4.0 had its *pH* increased to 12.0, and aliquots were taken every hour, from 1 to 5 h, their *pH* brought back to 4.0, and their optical absorption and emission registered (Fig. 4a and 5a and b). Similarly, part of the sample prepared at *pH* 12.0 had its *pH* decreased to 4.0, and aliquots were taken every hour, from 1 to 5 h, their *pH* brought back to *pH* 12.0, and their optical absorption and emission registered (Fig. 4b and 5c and d).

If we look at the samples kept at *pH* 4.0 for up to 5 h, it is evident that neither its optical absorption spectrum nor its emission change significantly, either measured at *pH* 4.0 (pink spectra in Fig. 4a and Fig. 5a and b), or measured at *pH* 12.0 (all but pink spectrum in Fig. 4b and Fig. 5c and d).

Contrarily, samples kept at *pH* 12.0 for a few hours, do show significant differences as compared to freshly prepared samples. For instance, the pink absorption spectrum in Fig. 4b is from a sample kept for 5 h at *pH* 12.0, and measured at the same *pH* value, 12.0. Clearly, the optical absorption spectrum is different from a freshly prepared sample (black line in Fig. 4b), or samples kept up to 5 h at *pH* 4.0 (all but pink spectrum in Fig. 4b). Similarly, the pink emission spectrum in Fig. 5c is from that sample kept for 5 h at *pH* 12.0, irradiated at 352 nm, and measured at *pH* 12.0. So, this emission band around 420 nm is certainly due to Barbaloin degradation products. Interestingly, if irradiated at 388 nm, Barbaloin emission spectrum is quite reproducible, even after the sample had been left for 5 h at *pH* 12.0 (pink spectrum in Fig. 5d), despite the presence of Barbaloin degradation products.

There is a clear isosbestic point in Fig. 4a, around 400 nm, probably indicating the decrease in Barbaloin concentration related to the increase of its degradation product. Products from Barbaloin degradation, when kept at high *pH*, are under investigation, but the study is out of the

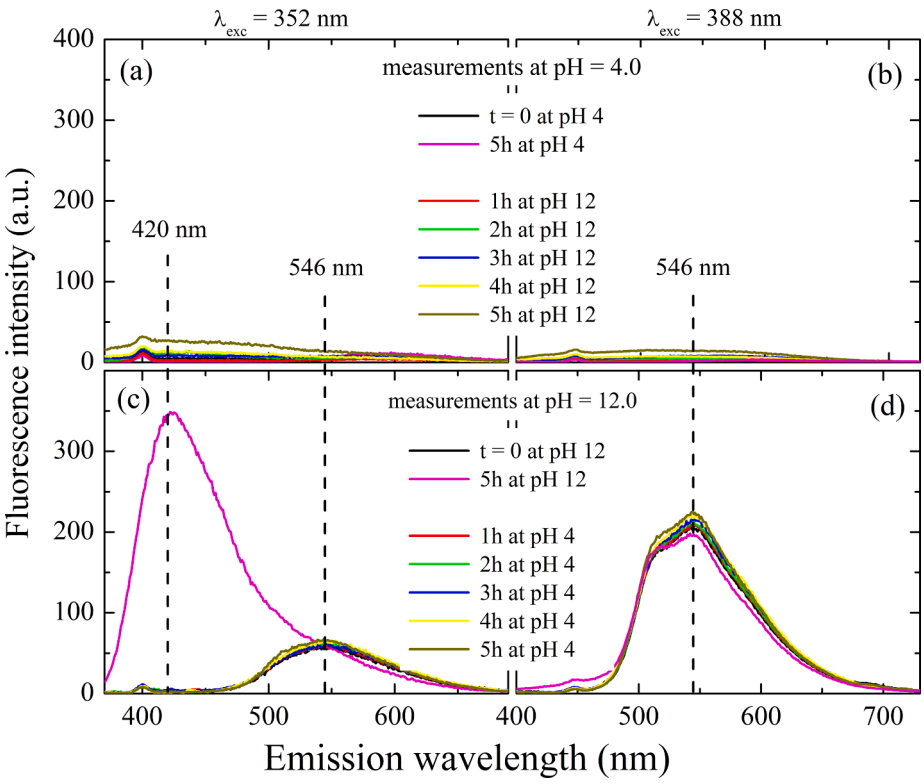

Fig. 5. Barbaloin (0.025 mM) fluorescence emission spectrum measured with samples at *pH* 4.0 (a and b) and *pH* 12.0 (c and d), irradiated at 352 nm (a and c) or at 388 nm (b and d). Spectra measured immediately after preparing the sample at *pH* 4 (black lines in a and b) and at *pH* 12.0 (black lines in c and d). Spectrum measured at *pH* 4.0 after incubating the sample for 5 h at *pH* 4 (pink lines in a and b), and spectrum measured at *pH* 12.0 after incubating the sample for 5 h at *pH* 12 (pink lines in c and d). The other spectra (lines red, green, blue, yellow and dark yellow) were obtained after incubating the sample for the given time at *pH* 12.0, and measured at *pH* 4.0 (a and b), or at *pH* 4.0 and measured at *pH* 12.0 (c and d).

scope of the present work.

Thus, our experiments show that there are significant changes in both absorption and emission spectra of Barbaloin when the sample is kept at *pH* 12.0 for a long time, but no changes were detected when the sample is kept up to 5 h at *pH* 4.0. Hence Barbaloin was found to be quite stable in solution at low *pH* value. Moreover, even at *pH* 12.0, at room temperature, Barbaloin seems to be reasonably stable for up to one hour with more than 97% of its initial concentration (compare black and red spectra in Fig. 4a and 5c and d).

The above discussion is essential for the understanding of the main differences found on the optical absorption and emission spectra obtained for Barbaloin along the two titration cycles, up- and down-titrations. For instance, we can focus at the emission band around 420 nm, that was clearly shown in Fig. 5c to be the product of Barbaloin degradation when kept in solution at high *pH* value. That emission band around 420 nm is present in the up-titration (Fig. 3a) but it is not present in the down-titration (Fig. 3c). That is due to the methodology used in this work and elsewhere [46 68 45]. As stated in Materials and methods, for the up-titration cycle, aliquots of a Barbaloin sample kept at *pH* 13 were added to the sample starting at *pH* 4.0. Hence, as shown above, the sample kept at *pH* 13 will have increasing amounts of degraded Barbaloin as time goes by. On the other hand, for the down-titration these intermediate *pH* samples were obtained by addition of small aliquots from a non-degraded Barbaloin sample kept at *pH* ~ 2. Important to stress that, along the down-titration, the time from the first spectrum measurement, at *pH* 13, to the measurement of the spectrum at *pH* around 10 was less than one hour, so the Barbaloin sample would not be degraded, as discussed above. Therefore, we adopted the down-titration spectra to perform the absorption and emission spectroscopic titration (ST) curves, to determine the pK_a values of Barbaloin in water.

It is important to note that the methodology employed here, with the use of a mixture of Barbaloin samples, at a fixed concentration, here 0.025 mM, at two extreme values of *pH*, to produce all samples at different *pH* values, is a very good choice when one wants to compare the optical spectrum of a molecule. That is the most reliable way of making sure that the spectrum you are measuring is due to a fixed molecular concentration. Moreover, this methodology allowed the clear distinction between optical absorption and fluorescence spectra due to Barbaloin degradation products and to protonation-deprotonation processes.

Indeed, in aqueous solution, Barbaloin is spontaneously susceptible to degradation depending on different factors such as *pH*, temperature, and light exposition. According to the literature [62 59 81 82], the major degradation products of Barbaloin are 10-Hydroxyaloins A and B, Elgonica-dimers A and B, Aloe-emodin, and other unknown substances. However, to the best of our knowledge, the optical characterization of the degradation products of Barbaloin in water is still an open question, out of the scope of the present work, deserving further investigation.

4.3. Spectroscopic titration analysis and pK_a values

Considering the above discussion, the spectroscopic titration (ST) analysis was performed with the optical absorption and emission spectra of Barbaloin at *pH* values above 8, (see section 3.1, Fig. 2a and 2c), obtained with the down-titration procedure only (Fig. 2d and Fig. 3c and d).

For the absorption spectrum, the values of the Barbaloin absorbance at two different wavelengths, 352 and 388 nm, were used for the ST (Fig. 6, left column), as they correspond, approximately, to the maximum of the absorption bands at low and high *pH* values, respectively (see dashed lines in Fig. 2c and d). As expected, the absorbance at 352 nm decreases, as the *pH* increases, while that at 388 nm increases.

As for the fluorescence emission, considering that the only relevant emission band for the *pH* titration is centered around 546 nm (see Fig. 3c and d), as previously discussed, this was our chosen wavelength for the fluorescence ST. The fluorescence intensity at 546 nm was plotted against the sample *pH* value for samples irradiated at 352 nm (black curves in Fig. 6, right column) and 388 nm (red curves in Fig. 6, right column).

The best values for the pK_a constants were determined from the best fits of Eq. (1) to the ST curves. As shown in Fig. 6, both absorption and fluorescence intensities were fitted using Eq. (1), with n = 1, 2 or 3, i.e.,

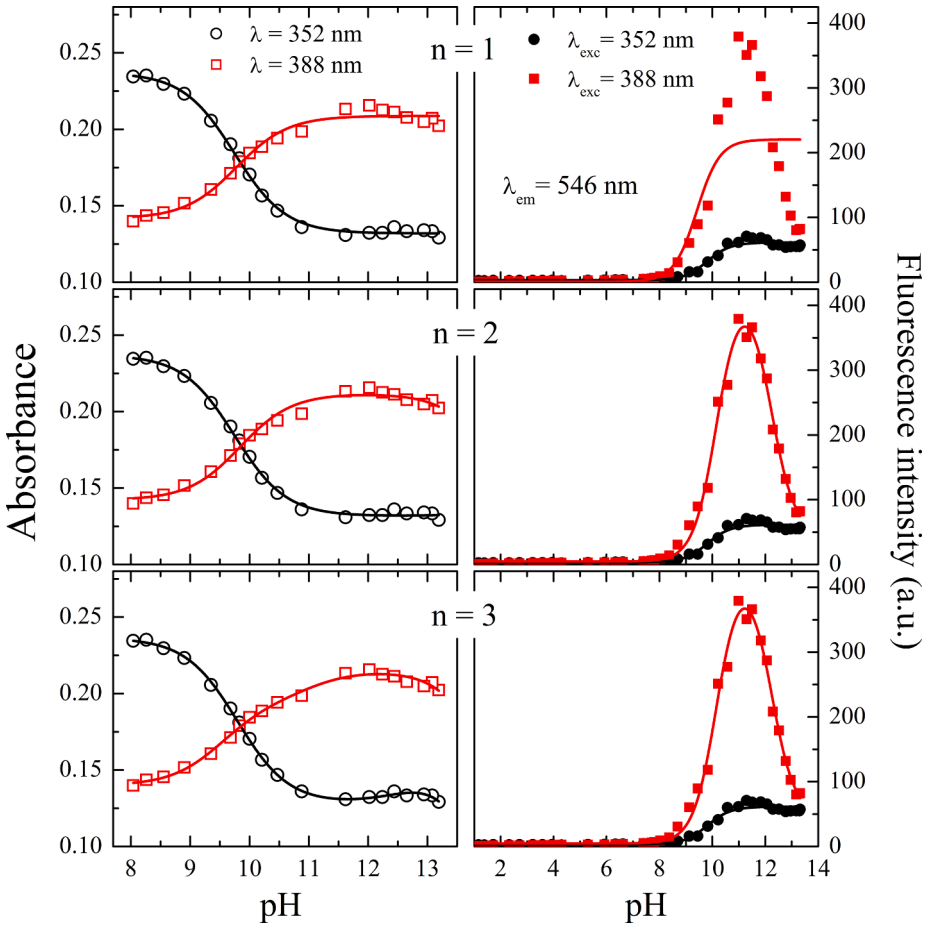

Fig. 6. Optical absorption and fluorescence *pH* titrations of Barbaloin. The intensity values, of Absorbance or fluorescence emission, are those shown in Fig. 2d (Absorbance) and Fig. 3c and d (fluorescence emission). The solid lines correspond to the best fits using Eq. (1) with one term (n = 1, top), two terms (n = 2, middle) and three terms (n = 3, bottom).

Table 1
The pK_a values for Barbaloin in water obtained from the best fitting of experimental data (Figures using the Eq (1) with one (n = 1), two (n = 2), and three (n = 3) terms for absorption and emission ST curves in both up-titration and down-titration.

	n = 1	n = 2		n = 3		
	pK_{a1}	pK_{a1}	pK_{a2}	pK_{a1}	pK_{a2}	pK_{a3}
Absorption ST curves						
352 nm	9.7 ± 0.1	9.7 ± 0.1	15.8 ± 0.2	9.7 ± 0.3	12.5 ± 0.1	16.7 ± 0.8
388 nm	9.8 ± 0.2	9.7 ± 0.1	15.9 ± 0.2	9.6 ± 0.1	12.5 ± 0.6	16.6 ± 0.5
Average 1	9.7 ± 0.2	9.7 ± 0.2	15.8 ± 0.3	9.6 ± 0.3	12.5 ± 0.6	16.6 ± 0.9
Emission ST curves						
546/352	9.1 ± 0.1	9.5 ± 0.1	12.1 ± 0.7	9.5 ± 0.1	13.2 ± 0.3	16.6 ± 0.7
546/388	8.9 ± 0.2	9.5 ± 0.1	12.0 ± 0.6	9.5 ± 0.2	12.4 ± 0.4	16.6 ± 0.5
Average 2	9.0 ± 0.2	9.5 ± 0.1	12.1 ± 0.9	9.5 ± 0.2	12.8 ± 0.5	16.6 ± 0.8
Overall average	9.3 ± 0.3	9.6 ± 0.2	14.0 ± 1.0	9.6 ± 0.6	12.6 ± 0.8	16.6 ± 1.2

assuming one, two or three decoupled and non-interacting protonation sites of Barbaloin in aqueous solution at the *pH* range examined (*pH* 8 – 13). Clearly, just with n = 1 (see Fig. 6) Eq. (1) cannot appropriately fit either the absorbance or the fluorescence ST curves. The use of n = 2 can fit both the absorbance and the emission ST curves (see n = 2 in Fig. 6). However, the best fits were obtained with n = 3, indicating the presence of three non-interacting protonation sites in Barbaloin (see Table 1).

Table 1 shows that the three pK_a values obtained for the fittings with n = 3, using either Barbaloin absorption or emission properties, were found to be rather similar. The similarities among the values obtained with the two spectroscopic techniques make the calculated values quite robust. However, the highest pK_a value is not reliable, as the titration performed here went to *pH* values up to 13.0 only. Hence, we can confidently state that Barbaloin displays at least two pK_a values from *pH* 8 to *pH* 13: $pK_{a1} = 9.6 \pm 0.6$ and $pK_{a2} = 12.6 \pm 0.8$, as shown in Table 1. Those values are the averages and errors for six different experiments, three for each optical technique (see Table 1). As expected, the values are not very different from those obtained with n = 2 (Table 1).

Hence, Barbaloin in water, at *pH* values from 2.0 to 13.0, loses two protons, going from the neutral form to the single and double deprotonated forms. This value of 9.6 ± 0.6 for the pK_{a1} is in good agreement with the value of 9.5 previously estimated by the MarvinSketch software package [61]. Interestingly, these two pK_a values found for Barbaloin in

aqueous solution are significantly higher than those obtained for Emodin ($pK_{a1} = 8.0 \pm 0.1$ and $pK_{a2} = 10.9 \pm 0.2$) [46], showing that the presence of the peripheral groups is relevant for the protonation/deprotonation processes of the anthraquinone.

4.4. Geometry optimization and assignment of protonation/deprotonation sites

To assign the Barbaloin protonation/deprotonation sites, and analyze the relative stability of its isomers, ab initio QM calculations were performed. Geometry optimization for the Barbaloin species in vacuum and in aqueous solution with the B3LYP/6–311++G(d,p) level of calculation were performed. In aqueous solution, the solvent effect was described by the polarizable continuum model (PCM) [74] with the same level of QM calculation. The optimized systems were the neutral form of Barbaloin (BBH, see Fig. 1) and all seven possible deprotonated hydroxyl forms, called x-BB^{-1}, with one single deprotonation site at position × = 1, 3, 8, 32, 33, 34 and 35 (see atomic numbering in Fig. 1). However, the geometry optimization of 35-BB^{-1} form (Barbaloin with deprotonation at position 35) showed a spontaneous tautomeric process involving the hydroxyl at position 34, resulting in the 34-BB^{-1} geometry. Therefore, only six stable anionic/deprotonated forms of Barbaloin were found: 1-BB^{-1}, 3-BB^{-1}, 8-BB^{-1}, 32-BB^{-1}, 33-BB^{-1} and 34-BB^{-1}. After finding the first deprotonation form with the lowest Gibbs free energy, all six possible second deprotonation forms, called x,y-BB^{-2}, were optimized: 1,3-BB^{-2}, 1,8-BB^{-2}, 1,32-BB^{-2}, 1,33-BB^{-2}, and 1,34-BB^{-2}. And finally, after finding the second deprotonation form with the lowest Gibbs free energy, all five possible third deprotonation forms, called x,y,z-BB^{-3}, were optimized: 1,34,3-BB^{-3}, 1,34,8-BB^{-3}, 1,34,32-BB^{-3}, 1,34,33-BB^{-3}, and 1,34,35-BB^{-3}. In that way, we found 17 stable structures in vacuum, being the neutral form (non-ionized) and 16 anionic/deprotonated forms of Barbaloin: (i) 6 are singly deprotonated, (ii) 5 are doubly deprotonated and (iii) 5 are triply deprotonated. The difference in electronic energies (ΔE) and in Gibbs free energies (ΔG) between the most stable forms of Barbaloin for the same quantity of deprotonation sites with the structures in vacuum and in aqueous solution are shown in Table 2.

The optimized geometry of the neutral form was found to have two intramolecular hydrogen bonds (IHB) with oxygen O9. The glucose group attached to the carbon C10 was shown to be strong enough to stabilize the structure of BBH with non-planar anthraquinone moiety. We found that all deprotonated forms of Barbaloin with one deprotonation site are stable at the B3LYP/6–311++G(d,p) level, except the 35-BB^{-1}, which exhibits a direct intramolecular proton transfer of position 35 to 34, by a spontaneous tautomeric interconversion to 34-BB^{-1}.

We observed that the IHB with oxygen O9 are stronger when changing from the neutral form to deprotonated forms 8-BB^{-1} or 1-BB^{-1}, as observed by the O···H distances: 1.69 Å for BBH and 1.55 Å for 8-BB^{-1} or 1-BB^{-1}. These stronger IHB are in agreement with the previous Emodin study [46].

In Table 2, comparing the difference in Gibbs free energies in vacuum, ΔG_g, among the most stable forms of Barbaloin with one deprotonation, 1-BB^{-1}, 3-BB^{-1}, 8-BB^{-1}, 32-BB^{-1}, 33-BB^{-1}, and 35-BB^{-1}, the isomer with deprotonation at position 1 is the most stable, compared with the others by 3.8 kcal/mol for 8-BB^{-1}, 20.5 kcal/mol for 3-BB^{-1}, 8.8 kcal/mol for 32-BB^{-1}, 6.4 kcal/mol for 33-BB^{-1}, and 0.48 kcal/mol for 35-BB^{-1}. The electronic energy, E_g and Gibbs free energy, G_g, in vacuum for the stable forms of Barbaloin, as well as the energies corrections (sum of zero-point, thermal, and enthalpy), are presented in the supplementary material (see Table 2SM). It is interesting to note that the difference in Gibbs free energies in vacuum between the 1-BB^{-1} and 34-BB^{-1} is less than 1 kcal/mol.

In aqueous solution, a significant change in the stabilization of the most stable forms with one deprotonation was also found, and the isomer 1-BB^{-1} is still the most stable form compared with the others by 3.3 kcal/mol for 8-BB^{-1}, 13.0 kcal/mol for 3-BB^{-1}, 9.1 kcal/mol for 32-BB^{-1}, 8.1 kcal/mol for 33-BB^{-1}, and 3.5 kcal/mol for 34-BB^{-1}. Consequently, this large ΔG_{aq} (greater than 3 kcal/mol) leads to an equilibrium system with only the isomer 1-BB^{-1} in aqueous solution at room temperature. Thus, this result leads to the assignment of the position 1 at the anthraquinone group for the first deprotonation of Barbaloin in aqueous solution. For doubly deprotonated isomers (divalent anionic forms), the isomer 1,34-BB^{-2} is more stable than the other isomers by 4.3 kcal/mol for 1,8-BB^{-2}, 10.7 kcal/mol for 1,3-BB^{-2}, 11.7 kcal/mol for 1,32-BB^{-2}, and 6.7 kcal/mol for 1,33-BB^{-2}. Thus, we assigned the position 34 at the glucose group for the second deprotonation of Barbaloin in water.

As mentioned above, due to the intramolecular proton transfer of position 34 to 35, the isomer 1,35-BB^{-2} was not found to be stable. For the triply deprotonated isomers (trivalent anionic forms), the isomer 1,34,8-BB^{-3} is also more stable than isomers 1,34,3-BB^{-3}, 1,34,32-BB^{-3}, 1,34,33-BB^{-3} and 1,34,35-BB^{-3} (see Table 2). Therefore, our results obtained with quantum mechanical calculations show that the first deprotonation of Barbaloin in water takes place at position 1 at the anthraquinone group, the second deprotonation at position 34, at the glucose group, and the third deprotonation at position 8 at the anthraquinone group.

Table 2
Difference in electronic energies (ΔE_g in kcal/mol) and in Gibbs free energies (ΔG_g in kcal/mol) between the most stable forms of Barbaloin in vacuum for the same quantity of deprotonation sites obtained using B3LYP/6–311++G(d,p) level of QM calculation. In aqueous solution, the difference in free energies (ΔG_{aq}) were obtained using the solvent described by PCM with the same level of calculation. Value of 0.00 for ΔG_{aq} means the most stable form.

X	ΔE_g	ΔG_g	ΔG_{aq}
1-BB^{-1}	**0.00**	**0.00**	**0.00**
8-BB^{-1}	4.96	3.81	3.26
3-BB^{-1}	21.36	20.48	13.02
32-BB^{-1}	6.79	8.78	9.05
33-BB^{-1}	5.78	6.42	8.11
34-BB^{-1}	−0.64	0.48	3.45
1,8-BB^{-2}	34.20	33.39	4.30
1,3-BB^{-2}	34.69	33.95	10.66
1,32-BB^{-2}	22.80	21.90	11.69
1,33-BB^{-2}	16.33	15.67	6.65
1,34-BB^{-2}	**0.00**	**0.00**	**0.00**
1,34,8-BB^{-3}	**0.00**	**0.00**	**0.00**
1,34,3-BB^{-3}	4.06	4.35	7.11
1,34,32-BB^{-3}	24.32	23.45	10.39
1,34,33-BB^{-3}	17.41	17.44	8.57
1,34,35-BB^{-3}	31.08	30.22	18.30

5. Conclusions

In the present study, we showed the dependence of the optical absorption and emission spectra of Barbaloin on the medium *pH*. Accordingly, that dependence was used to determine the acidity constants of the molecule, varying the medium *pH* from 2 to 13. The two calculated pK_a values are quite reliable, as very similar values were obtained using both spectroscopic techniques: $pK_{a1} = 9.6 \pm 0.6$ and $pK_{a2} = 12.6 \pm 0.8$. Interestingly, these acidity constants were found to be higher than those obtained for Emodin [46], a similar molecule which lacks the sugar moiety present in Barbaloin (Fig. 1).

For the titration measurements, the instability of Barbaloin in aqueous solution at high *pH* values was taken into consideration, analyzing the modifications caused on both absorption and fluorescence spectra due to molecular degradation. Thus, it was possible to well distinguish the changes caused either by protonation/deprotonation or degradation on the Barbaloin optical spectra. Barbaloin was found to be stable in aqueous solution at *pH* 4.0, but quite unstable if kept at *pH* 12.0 for a long time. However, even at *pH* 12.0, Barbaloin was found to be relatively stable at 25 °C for up to one hour.

Performing quantum mechanics calculations at B3LYP/6–311++G(d,p) level for non-ionized, singly, doubly, and triply deprotonated

forms of Barbaloin in vacuum and in aqueous solution, we conclude that the first deprotonation takes place at position 1, at the anthraquinone group, the second at position 34, at the glucose group, and the third at position 8, also at the anthraquinone group (see Fig. 1 for atomic numbering).

The determination of the pK_a values of Barbaloin is fundamental to the evaluation of the mechanism of action of this drug in different parts of an organism, as local *pH* values can vary quite significantly. Moreover, a future study of the biological activity of each Barbaloin isomer, together with the calculation presented here of the specific deprotonated sites, can be important for the design of more effective drugs.

CRediT authorship contribution statement

Fernanda Lima Matos: Investigation, Data curation, Software. **Evandro L. Duarte:** Investigation, Data curation, Software. **Gabriel S. V. Muniz:** Investigation, Data curation. **Erix Alexander Milán-Garcés:** Investigation, Data curation. **Kaline Coutinho:** Investigation, Data curation, Software, Resources. **M. Teresa Lamy:** Conceptualization, Methodology, Investigation, Resources. **Antonio R. da Cunha:** Conceptualization, Methodology, Investigation, Software, Writing – review & editing, Supervision.

Declaration of Competing Interest

The authors declare that they have no known competing financial interests or personal relationships that could have appeared to influence the work reported in this paper.

Data availability

Data will be made available on request.

Acknowledgement

We acknowledge the financial support of FAPESP (2017/25930-1; 2021/01593-1; 2021/09016-3) and the National Institute of Science and Technology Complex Fluids (INCT-FCx), financed by CNPq (141260/2017-3) and FAPESP (2014/50983-3 and 2018/20162-9). F.L.M. thanks FAPESP for an Undergraduate Scholarship, grant 2017/03910-9. M.T.L. and K.C. also thank CNPq for research fellowship.

Appendix A. Supplementary material

Supplementary data to this article can be found online at https://doi.org/10.1016/j.saa.2022.122020.

References

[1] Q. Groom, T. Reynolds, Barbaloin in *Aloe* Species, Planta Med. 53 (1987), https://doi.org/10.1055/s-2006-962735.
[2] T. Reynolds, A. Dweck, Aloe vera leaf gel: a review update, J. Ethnopharmacol. 68 (1999), https://doi.org/10.1016/S0378-8741(99)00085-9.
[3] D. Patel, K. Patel, V. Tahilyani, Barbaloin: a concise report of its pharmacological and analytical aspects, Asian Pac. J. Trop. Biomed. 2 (2012), https://doi.org/10.1016/S2221-1691(12)60239-1.
[4] S. Lazzara, A. Carrubba, E. Napoli, A. Culmone, A.C. Cangemi, A. Giovino, Increased illumination levels enhance biosynthesis of aloenin A and aloin B in Aloe arborescens Mill., but lower their per-plant yield, Ind. Crops Prod. 164 (2021), 113379, https://doi.org/10.1016/j.indcrop.2021.113379.
[5] Y. Gutterman, E. Chauser-Volfson, Peripheral defence strategy: variation of barbaloin content in the succulent leaf parts of Aloe arborescens Miller (Liliaceae), Bot. J. Linn. Soc. 132 (2000), https://doi.org/10.1111/j.1095-8339.2000.tb01219.x.
[6] X.L. Chang, C. Wang, Y. Feng, Z. Liu, Effects of heat treatments on the stabilities of polysaccharides substances and barbaloin in gel juice from Aloe vera Miller, J. Food Eng. 75 (2006), https://doi.org/10.1016/j.jfoodeng.2005.04.026.
[7] R.J. Sydiskis, D.G. Owen, J.L. Lohr, K.H. Rosler, R.N. Blomster, Inactivation of enveloped viruses by anthraquinones extracted from plants, Antimicrob. Agents Chemother. 35 (1991), https://doi.org/10.1128/AAC.35.12.2463.
[8] H.I. Abd-Alla, N.S. Abu-Gabal, A.Z. Hassan, M.M. El-Safty, N.M.M. Shalaby, Antiviral activity of Aloe hijazensis against some haemagglutinating viruses infection and its phytoconstituents, Arch. Pharm. Res. 35 (2012), https://doi.org/10.1007/s12272-012-0804-5.
[9] E.H. Kaparakou, C.D. Kanakis, M. Gerogianni, M. Maniati, K. Vekrellis, E. Skotti, P. A. Tarantilis, Quantitative determination of aloin, antioxidant activity, and toxicity of <scp> *Aloe vera* </scp> leaf gel products from Greece, J. Sci. Food Agric. 101 (2021) 414–423, https://doi.org/10.1002/jsfa.10650.
[10] R.Y.Y. Lam, A.Y.H. Woo, P.-S. Leung, C.H.K. Cheng, Antioxidant actions of phenolic compounds found in dietary plants on low-density lipoprotein and erythrocytes in vitro, J. Am. Coll. Nutr. 26 (2007), https://doi.org/10.1080/07315724.2007.10719606.
[11] Y. Sato, S. Ohta, M. Shinoda, Studies on Chemical Protectors against radiation. XXXI. protection Effects of Aloe arborescens on Skin Injury Induced by X-Irradiation, YAKUGAKU ZASSHI. 110 (1990), https://doi.org/10.1248/yakushi1947.110.11_876.
[12] V.K. Gupta, A. Kumar, M. de L. Pereira, N.J. Siddiqi, B. Sharma, Anti-Inflammatory and Antioxidative Potential of Aloe vera on the Cartap and Malathion Mediated Toxicity in Wistar Rats, Int. J. Environ. Res. Public Health. 17 (2020) 5177. https://doi.org/10.3390/ijerph17145177.
[13] Z. Huichun, F. Ruiqin, D. Xiaoguang, J. Linpei, Study of the Eu(III)-Barbaloin-Ctab System by Fluorescence and Determination of Barbaloin, Anal. Lett. 31 (1998), https://doi.org/10.1080/00032719808002820.
[14] H. El-Shemy, M. Aboul-Soud, A. Nassr-Allah, K. Aboul-Enein, A. Kabash, A. Yagi, Antitumor Properties and Modulation of Antioxidant Enzymes Activity by Aloe vera Leaf Active Principles Isolated via Supercritical Carbon Dioxide Extraction, Curr. Med. Chem. 17 (2010), https://doi.org/10.2174/092986710790112620.
[15] Q. Pan, H. Pan, H. Lou, Y. Xu, L. Tian, Inhibition of the angiogenesis and growth of Aloin in human colorectal cancer in vitro and in vivo, Cancer Cell Int. 13 (2013), https://doi.org/10.1186/1475-2867-13-69.
[16] M.Y. Li, Z. Liu, *In vitro* Effect of Chinese Herb Extracts on Caries-Related Bacteria and Glucan, J. Vet. Dent. 25 (2008), https://doi.org/10.1177/089875640802500403.
[17] K. Nakagomi, M. Yamamoto, H. Tanaka, N. Tomizuka, T. Masui, H. Nakazawa, Inhibition by Aloenin and Barbaloin of Histamine Release from Rat Peritoneal Mast Cells, Agric. Biol. Chem. 51 (1987), https://doi.org/10.1080/00021369.1987.10868254.
[18] Y. Gutterman, E. Chauser-Volfson, The distribution of the phenolic metabolites barbaloin, aloeresin and aloenin as a peripheral defense strategy in the succulent leaf parts of Aloe arborescens, Biochem. Syst. Ecol. 28 (2000), https://doi.org/10.1016/S0305-1978(99)00129-5.
[19] Y. Ishii, H. Tanizawa, Y. Takino, Studies of Aloe. V. Mechanism of Cathartic Effect. (4), Biol. Pharm. Bull. 17 (1994), https://doi.org/10.1248/bpb.17.651.
[20] J.C. Fishbein, J. Heilman, Advances in Molecular Toxicology, 11, Elsevier, London, 2017.
[21] H.-Z. Lee, S.-L. Hsu, M.-C. Liu, C.-H. Wu, Effects and mechanisms of aloe-emodin on cell death in human lung squamous cell carcinoma, Eur. J. Pharmacol. 431 (2001), https://doi.org/10.1016/S0014-2999(01)01467-4.
[22] H. Lee, C. Lin, W. Yang, W. Leung, S. Chang, Aloe-emodin induced DNA damage through generation of reactive oxygen species in human lung carcinoma cells, Cancer Lett. 239 (2006), https://doi.org/10.1016/j.canlet.2005.07.036.
[23] W. Jeon, Y.K. Jeon, M.J. Nam, Apoptosis by aloe-emodin is mediated through down-regulation of calpain-2 and ubiquitin-protein ligase E3A in human hepatoma Huh-7 cells, Cell Biol. Int. 36 (2012), https://doi.org/10.1042/CBI20100723.
[24] P.-L. Kuo, T.-C. Lin, C.-C. Lin, The antiproliferative activity of aloe-emodin is through p53-dependent and p21-dependent apoptotic pathway in human hepatoma cell lines, Life Sci. 71 (2002), https://doi.org/10.1016/S0024-3205(02)01900-8.
[25] P.-H. Huang, C.-Y. Huang, M.-C. Chen, Y.-T. Lee, C.-H. Yue, H.-Y. Wang, H. Lin, Emodin and Aloe-Emodin Suppress Breast Cancer Cell Proliferation through ER α Inhibition, Evidence-Based Complement. Altern. Med. (2013), https://doi.org/10.1155/2013/376123.
[26] J.-Q. Sui, K.-P. Xie, W. Zou, M.-J. Xie, Emodin Inhibits Breast Cancer Cell Proliferation through the ERα-MAPK/Akt-Cyclin D1/Bcl-2 Signaling Pathway, Asian Pacific J. Cancer Prev. 15 (2014), https://doi.org/10.7314/APJCP.2014.15.15.6247.
[27] K.-Y. Lin, Y.-H. Uen, Aloe-emodin, an anthraquinone, in vitro inhibits proliferation and induces apoptosis in human colon carcinoma cells, Oncol. Lett. 1 (2010), https://doi.org/10.3892/ol_00000096.
[28] P. Suboj, S. Babykutty, D.R. Valiyaparambil Gopi, R.S. Nair, P. Srinivas, S. Gopala, Aloe emodin inhibits colon cancer cell migration/angiogenesis by downregulating MMP-2/9, RhoB and VEGF via reduced DNA binding activity of NF-κB, Eur. J. Pharm. Sci. 45 (2012), https://doi.org/10.1016/j.ejps.2011.12.012.
[29] C. Tabolacci, S. Oliverio, A. Lentini, S. Rossi, A. Galbiati, C. Montesano, P. Mattioli, B. Provenzano, F. Facchiano, S. Beninati, Aloe-emodin as antiproliferative and differentiating agent on human U937 monoblastic leukemia cells, Life Sci. 89 (2011), https://doi.org/10.1016/j.lfs.2011.09.008.
[30] H. Chen, W. Hsieh, W. Chang, J. Chung, Aloe-emodin induced in vitro G2/M arrest of cell cycle in human promyelocytic leukemia HL-60 cells, Food Chem. Toxicol. 42 (2004), https://doi.org/10.1016/j.fct.2004.03.002.
[31] S.-H. Chen, K.-Y. Lin, C.-C. Chang, C.-L. Fang, C.-P. Lin, Aloe-emodin-induced apoptosis in human gastric carcinoma cells, Food Chem. Toxicol. 45 (2007), https://doi.org/10.1016/j.fct.2007.06.005.
[32] H.-Z. Lee, Protein kinase C involvement in aloe-emodin- and emodin-induced apoptosis in lung carcinoma cell, Br. J. Pharmacol. 134 (2001), https://doi.org/10.1038/sj.bjp.0704342.

[33] J.-G. Chung, Y.-C. Li, Y.-M. Lee, J.-P. Lin, K.-C. Cheng, W.-C. Chang, Aloe-emodin inhibited N-acetylation and DNA adduct of 2-aminofluorene and arylamine N-acetyltransferase gene expression in mouse leukemia L 1210 cells, Leuk. Res. 27 (2003), https://doi.org/10.1016/S0145-2126(03)00017-1.
[34] T. Pecere, M.V. Gazzola, C. Mucignat, C. Parolin, F.D. Vecchia, A. Cavaggioni, G. Basso, A. Diaspro, B. Salvato, M. Carli, G. Palù, Aloe-emodin Is a New Type of Anticancer Agent with Selective Activity against Neuroectodermal Tumors, Cancer Res. 60 (2000) 2800–2804. https://cancerres.aacrjournals.org/content/60/11/2800.
[35] L. Wasserman, S. Avigad, E. Beery, J. Nordenberg, E. Fenig, The Effect of aloe emodin on the proliferation of a new merkel carcinoma cell line, Am. J. Dermatopathol. 24 (2002), https://doi.org/10.1097/00000372-200202000-00003.
[36] H. Avila, J. Rivero, F. Herrera, G. Fraile, Cytotoxicity of a low molecular weight fraction from Aloe vera (Aloe barbadensis Miller) gel, Toxicon. 35 (1997), https://doi.org/10.1016/S0041-0101(97)00020-2.
[37] D.S. Alves, L. Pérez-Fons, A. Estepa, V. Micol, Membrane-related effects underlying the biological activity of the anthraquinones emodin and barbaloin, Biochem. Pharmacol. 68 (2004), https://doi.org/10.1016/j.bcp.2004.04.012.
[38] E.L. Duarte, T.R. Oliveira, D.S. Alves, V. Micol, M.T. Lamy, On the Interaction of the Anthraquinone Barbaloin with Negatively Charged DMPG Bilayers, Langmuir. 24 (2008), https://doi.org/10.1021/la703896w.
[39] A.K. Rivas-Sánchez, D.S. Guzmán-Hernández, M.T. Ramírez-Silva, M. Romero-Romo, M. Palomar-Pardavé, Quinizarin characterization and quantification in aqueous media using UV-VIS spectrophotometry and cyclic voltammetry, Dye. Pigment. 184 (2021), 108641, https://doi.org/10.1016/j.dyepig.2020.108641.
[40] D. Wang, G. Yang, X. Song, Determination of pKa values of anthraquinone compounds by capillary electrophoresis, Electrophoresis. 22 (2001) 464–469, https://doi.org/10.1002/1522-2683(200102)22:3<464::AID-ELPS464>3.0.CO;2-4.
[41] T. Pal, N.R. Jana, Emodin (1,3,8-trihydroxy-6-methylanthraquinone): a spectrophotometric reagent for the determination of beryllium(II), magnesium(II) and calcium(II), Analyst. 118 (1993) 1337, https://doi.org/10.1039/an9931801337.
[42] S.C. Nguyen, B.K. Vilster Hansen, S.V. Hoffmann, J. Spanget-Larsen, Electronic states of emodin and its conjugate base. Synchrotron linear dichroism spectroscopy and quantum chemical calculations, Chem. Phys. 352 (2008) 167–174, https://doi.org/10.1016/j.chemphys.2008.06.007.
[43] T. Philipova, C. Ivanova, Y. Kamdzhilov, M. Teresa Molina, Deprotonation and protonation studies of some substituted 1,4- and 9,10-anthraquinones, Dye. Pigment. 53 (2002) 219–227, https://doi.org/10.1016/S0143-7208(02)00016-5.
[44] D. Zarzeczańska, S. Ramotowska, A. Wcisło, I. Dąbkowska, P. Niedziałkowski, T. Ossowski, In pursuit of the ideal chromoionophores (part I): pH-spectrophotometric characteristics of aza-12-crown-4 ethers substituted with an anthraquinone moiety, Dye. Pigment. 130 (2016) 273–281, https://doi.org/10.1016/j.dyepig.2016.03.014.
[45] T. Ossowski, M.O.F. Goulart, F.C. de Abreu, A.E.G. Sant Ana, P.R.B. Miranda, C. de O. Costa, A. Liwo, P. Falkowski, D. Zarzeczanska, Determination of the pKa values of some biologically active and inactive hydroxyquinones, J. Braz. Chem. Soc. 19 (2008) 175–183. https://doi.org/10.1590/S0103-50532008000100025.
[46] A.R. da Cunha, E.L. Duarte, M.T. Lamy, K. Coutinho, Protonation/deprotonation process of Emodin in aqueous solution and pKa determination: UV/Visible spectrophotometric titration and quantum/molecular mechanics calculations, Chem. Phys. 440 (2014), https://doi.org/10.1016/j.chemphys.2014.06.009.
[47] Z. El Rassi, Carbohydrate analysis : high performance liquid chromatography and capillary electrophoresis, Elsevier, Amsterdam, 1995.
[48] N.E. Safronov, T.O. Fomin, A.S. Minin, L. Todorov, I. Kostova, E. Benassi, N. P. Belskaya, 5-Amino-2-aryl-1,2,3-triazol-4-carboxylic acids: synthesis, photophysical properties, and application prospects, Dye. Pigment. 178 (2020), 108343, https://doi.org/10.1016/j.dyepig.2020.108343.
[49] R.F. Cookson, Determination of acidity constants, Chem. Rev. 74 (1974) 5–28, https://doi.org/10.1021/cr60287a002.
[50] D. Snigur, M. Fizer, A. Chebotarev, O. Lukianova, O. Zhukovetska, Spectroscopic and computational studies of erythrosine food dye protonation in aqueous solution, Dye. Pigment. 198 (2022), 110028, https://doi.org/10.1016/j.dyepig.2021.110028.
[51] M. Shamsipur, Quantitative structure–property relationship study of acidity constants of some 9,10-anthraquinone derivatives using multiple linear regression and partial least-squares procedures, Talanta. 54 (2001) 1113–1120, https://doi.org/10.1016/S0039-9140(01)00374-5.
[52] Y. Marunaka, The Proposal of Molecular Mechanisms of Weak Organic Acids Intake-Induced Improvement of Insulin Resistance in Diabetes Mellitus via Elevation of Interstitial Fluid pH, Int. J. Mol. Sci. 19 (2018) 3244, https://doi.org/10.3390/ijms19103244.
[53] D. Pandey, T. Malik, R. Banik, Quantitative estimation of barbaloin in Aloe vera and its commercial formulations by using HPTLC, Int. J. Med. Aromat. Plants. 2 (2012) 420–427.
[54] K. Logaranjan, T. Devasena, K. Pandian, Quantitative Detection of Aloin and Related Compounds Present in Herbal Products and Aloe vera Plant Extract Using HPLC Method, Am. J. Anal. Chem. 04 (2013), https://doi.org/10.4236/ajac.2013.410071.
[55] D.K. Pandey, S. Parida, A. Dey, Comparative HPTLC analysis of bioactive marker barbaloin from in vitro and naturally grown Aloe vera, Rev. Bras. Farmacogn. 26 (2016), https://doi.org/10.1016/j.bjp.2015.08.016.
[56] M. Wichtl, Herbal Drugs and Phytopharmaceuticals, 3rd expanded and completely rev. ed,, CRC Press, Boca Raton, FL, 2004.
[57] F. Yang, Y. Cao, H. Yu, Y. Guo, Y. Cheng, H. Qian, W. Yao, Y. Xie, Transformation and degradation of barbaloin in aqueous solutions and aloe powder under different processing conditions, Food Biosci. 43 (2021), 101279, https://doi.org/10.1016/j.fbio.2021.101279.
[58] L. Lucini, M. Pellizzoni, G. Pietro Molinari, Stability of the main Aloe fractions and Aloe-based commercial products under different conditions, Agrochimica. LV (2011) 288–296.
[59] J.A. Gutierrez-Uribe, L.M.L. Nollet, Phenolic Compounds in Food: Characterization and Analysis, CRC Press, Boca Raton, 2018.
[60] Q. Xia, J. Yin, P. Fu, M. Boudreau, Photo-irradiation of Aloe vera by UVA—Formation of free radicals, singlet oxygen, superoxide, and induction of lipid peroxidation☆, Toxicol. Lett. 168 (2007) https://doi.org/10.1016/j.toxlet.2006.11.015.
[61] P. Csizmadia, MarvinSketch and MarvinView: molecule applets for the World Wide Web, (1999).
[62] W.-J. Ding, X.-F. Wu, J.-S. Zhong, J.-Z. Wan, Effects of temperature, pH and light on the stability of aloin A and characterisation of its major degradation products, Int. J. Food Sci. Technol. 49 (2014), https://doi.org/10.1111/ijfs.12500.
[63] D.I. Sánchez-Machado, J. López-Cervantes, M.F. Mariscal-Domínguez, P. Cruz-Flores, O.N. Campas-Baypoli, E.U. Cantú-Soto, A. Sanches-Silva, An HPLC Procedure for the Quantification of Aloin in Latex and Gel from Aloe barbadensis Leaves, J. Chromatogr. Sci. 55 (2017), https://doi.org/10.1093/chromsci/bmw179.
[64] P. Hohenberg, W. Kohn, Inhomogeneous Electron Gas, Phys. Rev. 136 (1964) B864–B871, https://doi.org/10.1103/PhysRev.136.B864.
[65] J. Seminario, Recent developments and applications of modern densityfunctional theory, theoretical and computational chemistry, ElsevierScience B.V, Oxford, 1996, p. 1996.
[66] A. Mendonça, A.C. Rocha, A.C. Duarte, E.B.H. Santos, The inner filter effects and their correction in fluorescence spectra of salt marsh humic matter, Anal. Chim. Acta. 788 (2013), https://doi.org/10.1016/j.aca.2013.05.051.
[67] G.S. Vignoli Muniz, M.C. Souza, E.L. Duarte, M.T. Lamy, Comparing the interaction of the antibiotic levofloxacin with zwitterionic and anionic membranes: calorimetry, fluorescence, and spin label studies, Biochim. Biophys. Acta - Biomembr. 1863 (2021), https://doi.org/10.1016/j.bbamem.2021.183622.
[68] A. Onufriev, D.A. Case, G.M. Ullmann, A Novel View of pH Titration in Biomolecules, Biochemistry 40 (2001) 3413–3419, https://doi.org/10.1021/bi002740q.
[69] R.G. Parr, Y. Weitao, Density-Functional Theory of Atoms and Molecules, Oxford University Press, USA, 1994. http://www.amazon.com/Density-Functional-Molecules-International-Monographs-Chemistry/dp/0195092767/ref=sr_1_1?ie=UTF8&s=books&qid=1279096906&sr=1-1.
[70] A.D. Becke, Density-functional thermochemistry. III. The role of exact exchange, J. Chem. Phys. 98 (1993) 5648–5652. https://doi.org/10.1063/1.464913.
[71] Y. Imamura, T. Otsuka, H. Nakai, Description of core excitations by time-dependent density functional theory with local density approximation, generalized gradient approximation, meta-generalized gradient approximation, and hybrid functionals, J. Comput. Chem. 28 (2007) 2067–2074, https://doi.org/10.1002/jcc.20724.
[72] R. Ditchfield, W.J. Hehre, J.A. Pople, S.-C.-O. Methods, Ix., An extended gaussian-type basis for molecular-orbital studies of organic molecules, J. Chem. Phys. 54 (1971) 724–728, https://doi.org/10.1063/1.1674902.
[73] Z. Machatová, Z. Barbieriková, P. Poliak, V. Jančovičová, V. Lukeš, V. Brezová, Study of natural anthraquinone colorants by EPR and UV/vis spectroscopy, Dye. Pigment. 132 (2016) 79–93, https://doi.org/10.1016/j.dyepig.2016.04.046.
[74] S. Miertuš, E. Scrocco, J. Tomasi, Electrostatic interaction of a solute with a continuum. A direct utilizaion of AB initio molecular potentials for the prevision of solvent effects, Chem. Phys. 55 (1981) 117–129, https://doi.org/10.1016/0301-0104(81)85090-2.
[75] M.J. Frisch, G.W. Trucks, H.B. Schlegel, G.E. Scuseria, M.A. Robb, J.R. Cheeseman, G. Scalmani, V. Barone, B. Mennucci, G.A. Petersson, H. Nakatsuji, M. Caricato, X. Li, H.P. Hratchian, A.F. Izmaylov, J. Bloino, G. Zheng, J.L. Sonnenberg, M. Hada, M. Ehara, K. Toyota, R. Fukuda, J. Hasegawa, M. Ishida, T. Nakajima, Y. Honda, O. Kitao, H. Nakai, T. Vreven, J.A. Montgomery Jr., J.E. Peralta, F. Ogliaro, M. Bearpark, J.J. Heyd, E. Brothers, K.N. Kudin, V.N. Staroverov, R. Kobayashi, J. Normand, K. Raghavachari, A. Rendell, J.C. Burant, S.S. Iyengar, J. Tomasi, M. Cossi, N. Rega, J.M. Millam, M. Klene, J.E. Knox, J.B. Cross, V. Bakken, C. Adamo, J. Jaramillo, R. Gomperts, R.E. Stratmann, O. Yazyev, A.J. Austin, R. Cammi, C. Pomelli, J.W. Ochterski, R.L. Martin, K. Morokuma, V.G. Zakrzewski, G.A. Voth, P. Salvador, J.J. Dannenberg, S. Dapprich, A.D. Daniels, Ö. Farkas, J.B. Foresman, J. V Ortiz, J. Cioslowski, D.J. Fox, Gaussian~09, (n.d.).
[76] W.G. Wamer, P. Vath, D.E. Falvey, In vitro studies on the photobiological properties of aloe emodin and aloin A, Free Radic. Biol. Med. 34 (2003), https://doi.org/10.1016/S0891-5849(02)01242-X.
[77] A.C.F. Xavier, M.L. de Moraes, M. Ferreira, Immobilization of aloin encapsulated into liposomes in Layer-by-layer films for transdermal drug delivery, Mater. Sci. Eng. C. 33 (2013), https://doi.org/10.1016/j.msec.2012.12.021.
[78] S.R. Kavitha, M. Umadevi, S.R. Janani, T. Balakrishnan, R. Ramanibai, Fluorescence quenching and photocatalytic degradation of textile dyeing waste water by silver nanoparticles, Spectrochim, Acta Part A Mol. Biomol. Spectrosc. 127 (2014), https://doi.org/10.1016/j.saa.2014.02.076.
[79] M. Rastogi, A. Chauhan, H.S. Kushwaha, R.V. Kumar, R. Vaish, Reaping the benefits of ferroelectricity in selectively precipitated lithium niobate microcrystals in silica matrix for photocatalysis, Appl. Phys. Lett. 109 (2016), https://doi.org/10.1063/1.4970774.

[80] E.S. Da Silva, H.D. Burrows, P. Wong-Wah-Chung, M. Sarakha, β-Cyclodextrin as a photostabilizer of the plant growth regulator 2-(1-naphthyl) acetamide in aqueous solution, J. Incl. Phenom. Macrocycl. Chem. 79 (2014), https://doi.org/10.1007/s10847-013-0355-5.

[81] T. Shindo, H. Ushiyama, K. Kan, S. Uehara, K. Yasuda, I. Takano, K. Saito, Contents of Barbaloin-related Compounds in Aloe Drinks and Their Change during Storage, J. Food Hyg. Soc. Japan (Shokuhin Eiseigaku Zasshi) 43 (2002), https://doi.org/10.3358/shokueishi.43.122.

[82] J.-H. Chung, J.-C. Cheong, J.-Y. Lee, H.-K. Roh, Y.-N. Cha, Acceleration of the alcohol oxidation rate in rats with aloin, a quinone derivative of Aloe, Biochem. Pharmacol. 52 (1996), https://doi.org/10.1016/S0006-2952(96)00514-X.